Efficient photocatalytic degradation of tetracycline hydrochloride by $Cu_2O/BiVO_4$ p-n heterostructure

J. X. Wang[a], L. J. Mao[a], Y. J. Duan[a], K. Lei[a], X. H. Zeng[a], Y. Sun[a,b] , T. Li[a,b*]
[a]*School of Mechanical Engineering, Chengdu University, Chengdu, 610106, China*
[b]*Sichuan Province Engineering Technology Research Center of Powder Metallurgy, Chengdu, 610106, China*

Star-like $BiVO_4$ and Cu_2O nanocubes were prepared by hydrothermal method and chemical reduction, respectively, and $Cu_2O/BiVO_4$ p-n heterojunction with different mass ratios of Cu_2O to $BiVO_4$ (3:1, 1:1, 1:3) were synthesized via facile physical mixing. The as-synthesized samples were characterized by X-ray powder diffraction (XRD), scanning electron microscopy (SEM), UV-vis diffuse reflection spectroscopy (DRS) and X-ray photoelectron spectroscopy (XPS). The photocatalytic performance of the $Cu_2O/BiVO_4$ composites was evaluated by degradation of tetracycline hydrochloride (TC) under simulated solar illumination. Owing to the fast charge transfer between n-type $BiVO_4$ and p-type Cu_2O, $Cu_2O/BiVO_4$ composites exhibited superior photocatalytic activity. When the mass ratio of Cu_2O to $BiVO_4$ was 1:3, the highest degradation efficiency of TC reached 78.9% within 24 min.

(Received January 12, 2024; Accepted April 8, 2024)

Keywords: $Cu_2O/BiVO_4$, p-n heterojunction, Antibiotics, Photocatalysis

1. Introduction

Nowadays, tetracycline antibiotics are widely applied in the prevention and treatment of animal diseases. However, the excessive use of antimicrobial agents has caused the accumulation of these compounds in the environment, which can induce negative impact to human health [1,2]. Semiconductor photocatalysis using solar energy is a green technology that is critical for the degradation of antibiotics. Among various photocatalysts [3-5], bismuth vanadate ($BiVO_4$), a n-type semiconductor, has attracted much attention for pollutant decomposition owing to suitable bandgap of 2.4 eV and excellent chemical stability [6]. However, the rapid recombination rate and slow transfer rate of photogenerated charge carriers greatly restricted the photocatalytic performance of $BiVO_4$ [7]. Therefore, it is necessary to modify $BiVO_4$ to improve the photocatalytic activity.

Previous literatures [8-12] have reported that coupling $BiVO_4$ with other semiconductors is an effective method to promote the separation of photoinduced electron-hole pairs. Natda Wetchakun et al. [13] prepared $BiVO_4/CeO_2$ nanocomposites using homogeneous precipitation

* Corresponding author: litao@cdu.edu.cn
https://doi.org/10.15251/DJNB.2024.192.539

and hydrothermal technique and the degradation efficiency of methylene blue reached 78.9% within 30 min. Abd-Rabboh et al. [14] synthesized $BiVO_4/TiO_2$ heterojunction via sonochemical route and the composites exhibited higher photocatalytic activity for Rhodamine B degradation. In particular, the formation of p-n heterojunction has been verified that can greatly facilitate the separation of photoinduced carriers due to the presence of a built-in electric fields at the interfaces [15]. As a p-type semiconductor, Cu_2O has been regarded as a promising photocatalyst because of its low cost, narrow bandgap of about 2.1 eV, and no toxicity properties [16]. Thus, Cu_2O is an appropriate p-type semiconductor for the construction of p-n heterojunction with $BiVO_4$.

In this study, cubic Cu_2O was synthesized by the chemical reduction of copper sulfate using glucose. A novel star-like structure of $BiVO_4$ was prepared by the hydrothermal method. The $BiVO_4/Cu_2O$ heterojunctions with different mass ratios of Cu_2O were synthesized via a facile physical mixing method. The photocatalytic performance of the $Cu_2O/BiVO_4$ composites was evaluated by degradation of TC solutions under simulated solar illumination. Furthermore, the photocatalytic degradation mechanism of TC over $Cu_2O/BiVO_4$ photocatalyst was discussed in detail.

2. Experimental

2.1. Synthesis of catalysts

The synthesis of Cu_2O was carried out under 70 ℃ water bath conditions with stirring during the whole process. Firstly, 30 mL of 3.0 M NaOH solution was added into 300 mL of 0.1 M $CuSO_4$. Then 18 mmol of glucose was added to the above solution and kept stirring for 90 min. The products were collected by centrifugation, washed with deionized water, and dried in a vacuum oven.

Star-like $BiVO_4$ with four angles was prepared in accordance with the previous literature [17]. 120 mg of $Bi(NO_3)_3 \cdot 5H_2O$ and 200 mg of $Na_3VO_4 \cdot 12H_2O$ were dissolved in 80 mL deionized water. After fully mixing, the mixture was transferred into a Teflon-lined autoclave (100 mL). The hydrothermal reaction was subsequently conducted at 160 °C for 8 h. The products were washed with deionized water and ethanol for three times. After drying at 60 °C, the star-like $BiVO_4$ nanocrystal powder was obtained.

The $Cu_2O/BiVO_4$ composites were fabricated via a physical mixing method. In brief, a certain amount of Cu_2O and $BiVO_4$ was added into ethanol with continuous stirring, and then the suspension was dried to obtain $Cu_2O/BiVO_4$ composites. The $Cu_2O/BiVO_4$ catalysts were synthesized at various mass ratios of Cu_2O to $BiVO_4$ (3:1, 1:1, 1:3) and were denoted as Cu_2O:$BiVO_4$ (3:1), Cu_2O:$BiVO_4$ (1:1) and Cu_2O:$BiVO_4$ (1:3), respectively.

2.2. Characterization

The crystal structure of samples was characterized by X-ray diffraction (XRD, Rigaku Ultima IV). The microstructure and morphology characterization of photocatalyst were performed by scanning electron microscopy (SEM, ZEISS Gemini SEM 300). Ultraviolet-visible diffuse reflectance spectra (DRS) were recorded on a TU-1901 spectrometer. The surface composition of catalysts was detected by X-ray photoelectron spectroscopy (XPS, Thermo

Scientific K-Alpha). The valence band (VB) of samples was studied by XPS using Thermo Scientific ESCALAB Xi+ instrument.

2.3. Photocatalytic experiments

The light source was a 500 W Xenon lamp with a cut-off filter (AM 1.5, 100 mW/cm^2). In a typical procedure, 40 mg of photocatalyst was dispersed in 100 mL TC solution (20 mg/L). The suspension was stirred in the dark for 45 min to achieve the adsorption-desorption equilibrium. During the photocatalytic degradation, the suspension was taken from the reactor at a certain time interval and centrifuged. The concentration of TC was measured by the UV-vis spectrophotometer (TU-1901).

3. Results and discussion

XRD patterns of the as-prepared $BiVO_4$, Cu_2O and Cu_2O:$BiVO_4$ (1:3) catalysts are shown in Fig. 1. For pure Cu_2O, the diffraction peaks at 2θ = 29.6°, 36.4°, 42.3°, and 61.3° are assigned to the (110), (111), (200) and (220) planes of Cu_2O (JCPDS No. 05-0667) [18,19], respectively. In the XRD pattern of $BiVO_4$, the peaks match well with those of monoclinic $BiVO_4$ (JCPDS No. 14-0688). Furthermore, the diffraction peaks of the composites are only composed of the characteristic peaks of monoclinic $BiVO_4$ which is mainly attributed to the low amount of Cu_2O utilized in the synthesis of the composites.

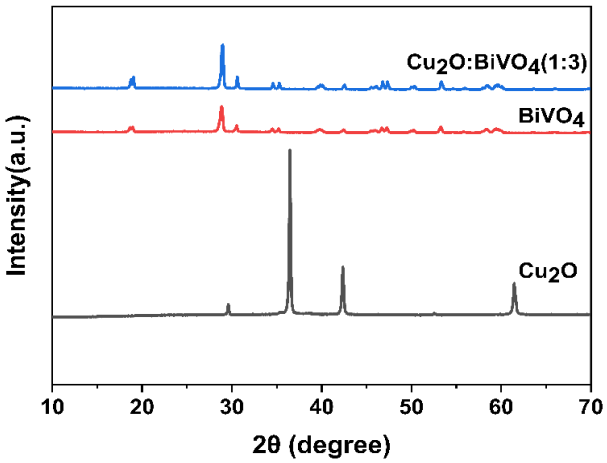

Fig. 1. XRD patterns of the as-prepared $BiVO_4$, Cu_2O and Cu_2O:$BiVO_4$ (1:3) composites.

The microstructure of the samples was characterized by SEM and the results are illustrated in Fig. 2. As shown in Fig. 2a, the prepared $BiVO_4$ exhibits star-like structure with particle size of 2-4 μm and thickness of about 100 nm. In Fig. 2b and Fig. 2c, Cu_2O nanocubes show well-defined and uniform shape with (100) facets and the length of the edges of nanocubes is around 600 nm. For the Cu_2O/$BiVO_4$ composites with different mass ratios (Fig. 2d-f), Cu_2O nanocubes are well dispersed with $BiVO_4$ particles. As the proportion of Cu_2O in the composites increases, more cubic Cu_2O nanoparticles can be observed in the SEM images.

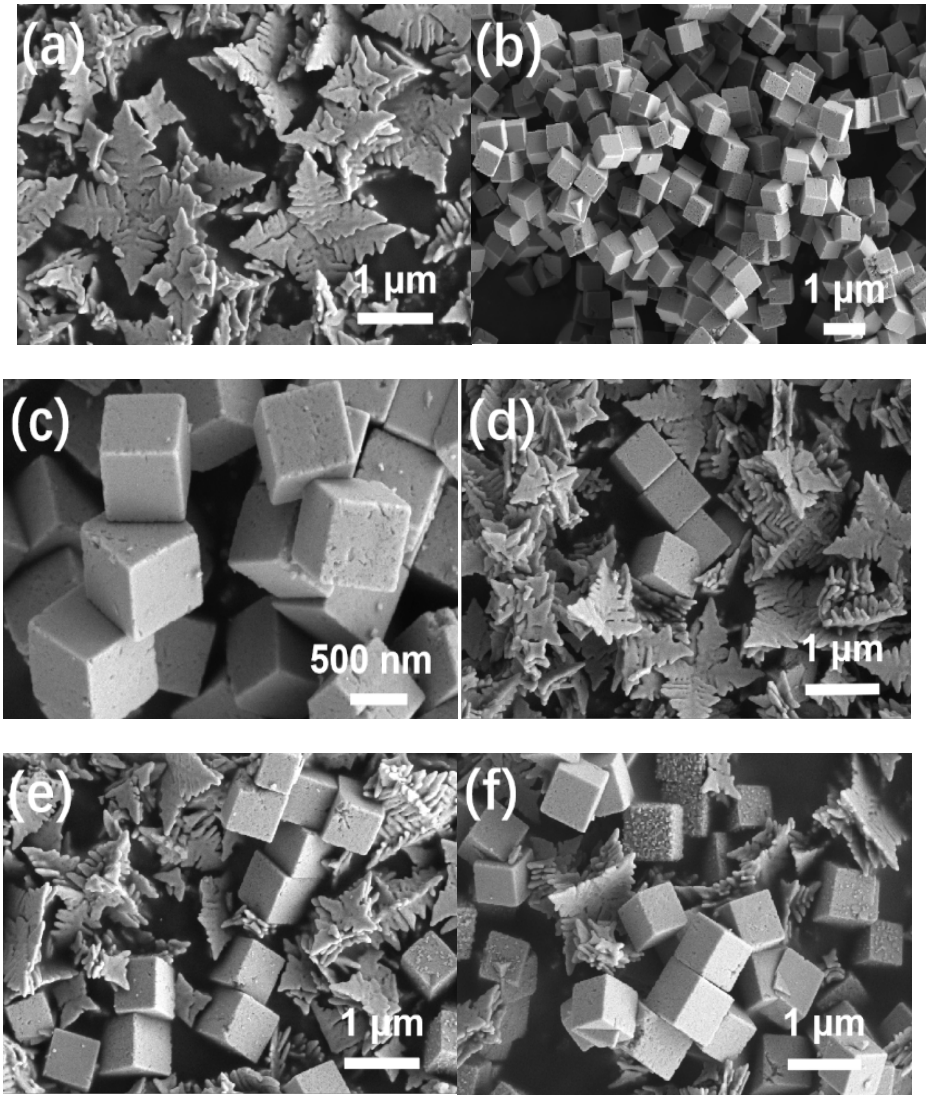

Fig. 2. The SEM images of (a) $BiVO_4$, (b, c) Cu_2O, (d) Cu_2O:$BiVO_4$ (1:3), (e) Cu_2O:$BiVO_4$ (1:1) and (f) Cu_2O:$BiVO_4$ (3:1).

Fig. 3a shows XPS full survey spectrum of Cu_2O:$BiVO_4$ (1:3) sample, indicating the existence of Cu, Bi, V, O and C elements. In Fig. 3b, two main peaks at 932.3 and 951.9 eV are assigned to the peaks of Cu $2p_{3/2}$ and Cu $2p_{1/2}$, respectively, which are indexed to the lattice of Cu_2O [20,21]. In addition, three small peaks at 935.0 eV (Cu $2p_{3/2}$), 941 eV (Cu $2p_{1/2}$) and 945.0 eV (Cu $2p_{1/2}$) correspond to Cu^{2+} [22-24], which may be attributed to the partial surface oxidation on the facets of Cu_2O. For Bi 4f (Fig. 3c), two peaks located at the binding energies of 158.5 and 163.8 eV are indexed to Bi $4f_{7/2}$ and Bi $4f_{5/2}$, respectively, indicating the presence of Bi^{3+} [25]. The peaks at the binding energies of 516.2 and 523.6 eV in the V 2p spectra (Fig. 3d) can be assigned to V $2p_{3/2}$ and V $2p_{1/2}$, respectively, confirming the presence of V^{5+} in the sample [26]. In the XPS spectrum of O 1s (Fig. 3e), the predominant peak at the binding energy of 530.4 eV is ascribed to lattice O (Bi-O and Cu-O), and the weaker peak at the binding energy of 531.8 eV is

attributed to adsorbed O (the oxygen adsorbed at the surface) [27-29]. Based on the XRD and XPS results, it is reasonable to confirm that the as-prepared composites are composed of Cu_2O and $BiVO_4$.

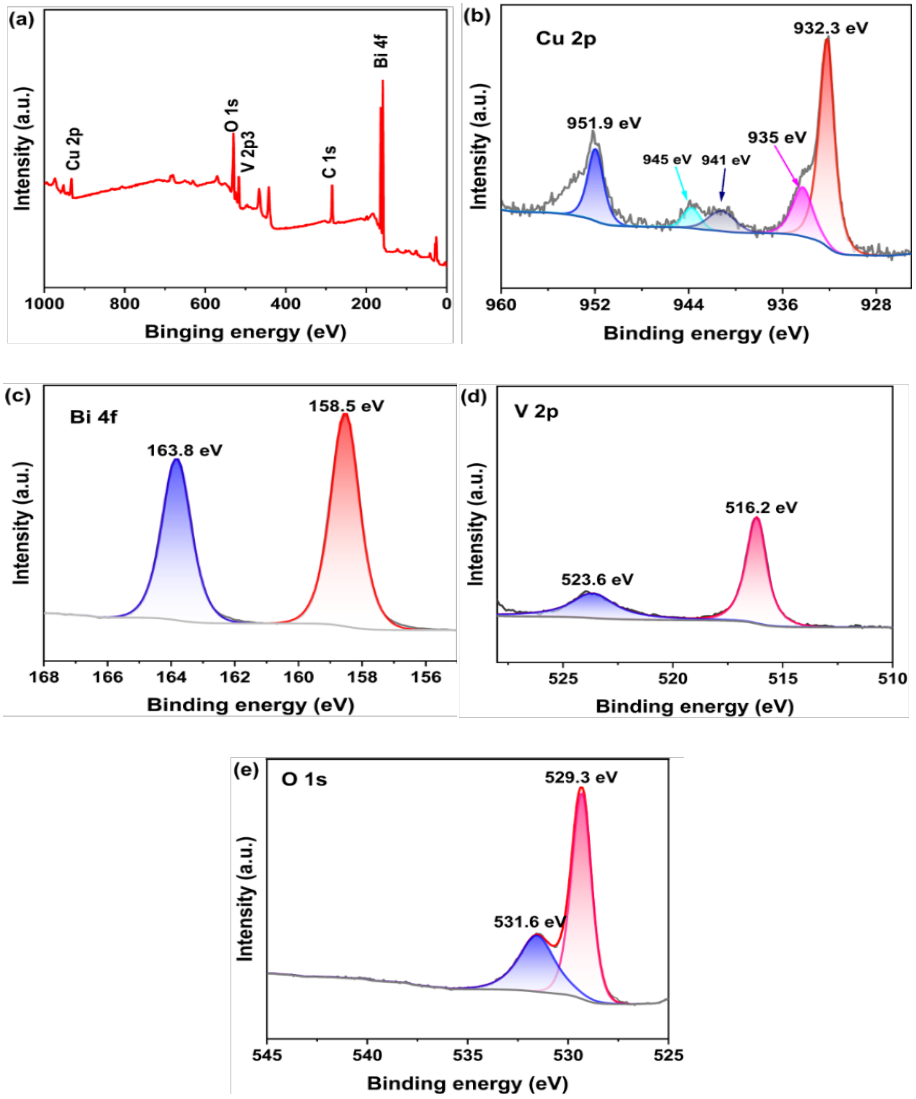

Fig. 3. XPS spectra of Cu_2O:$BiVO_4$ (1:3): (a) full survey, (b) Cu 2p, (c) Bi 4f, (d) V 2p, and (e) O 1s.

The UV-vis diffuse reflectance spectra of $BiVO_4$, Cu_2O, and Cu_2O:$BiVO_4$ (1:3) are shown in Fig. 4a. The absorption edges of $BiVO_4$, Cu_2O, and Cu_2O:$BiVO_4$ (1:3) are approximately 512 nm, 620 nm, and 545 nm, respectively. Obviously, $Cu_2O/BiVO_4$ composites show stronger light absorption than that of pure $BiVO_4$ in the visible region. Therefore, it can be inferred that $Cu_2O/BiVO_4$ samples could be excited to generate more electron-hole pairs under the same visible light illumination, which is beneficial to improve photocatalytic activity. Furthermore, the bandgap energy (Eg) values of $BiVO_4$ and Cu_2O are obtained as 2.51 and 2.12 eV, respectively, using Tauc plot method (Fig. 4b) [30].

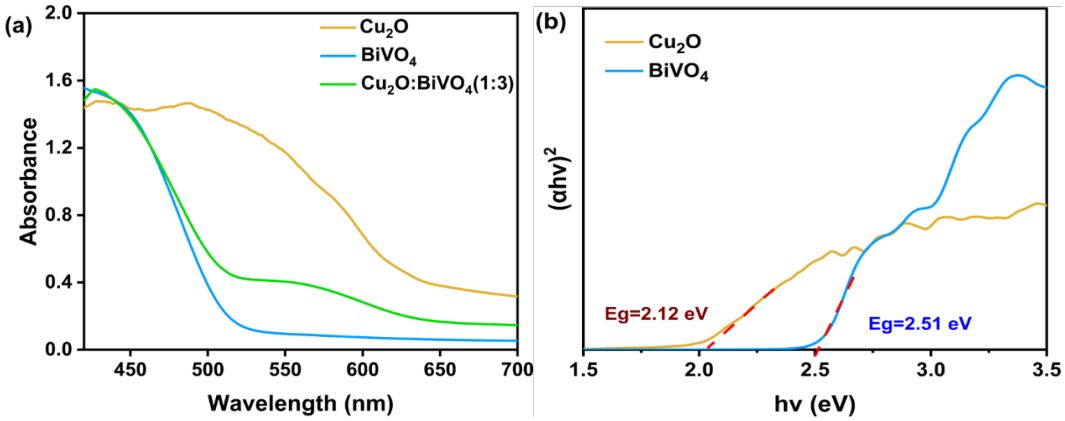

Fig. 4. (a) UV-vis diffuse reflectance spectra of $BiVO_4$, Cu_2O and Cu_2O:$BiVO_4$ (1:3); (b) the bandgap of $BiVO_4$ and Cu_2O.

Fig. 5a and Fig. 5b show the valence band (VB) positions of Cu_2O and $BiVO_4$. According to the following formula [31], the actual VB values of Cu_2O and $BiVO_4$ can be calculated as 1.17 and 1.64 eV.

$$E_{NHE} = \phi\square\ E_{VL}\square\square4$$

where E_{NHE} is potential of normal hydrogen electrode, ϕ is electron work function of the instrument (4.6 eV) and E_{VL} is potential of vacuum level, respectively. Based on the bandgap and VB results above, the conduction band (CB) values of Cu_2O and $BiVO_4$ are determined as -0.95 and -0.87 eV, respectively.

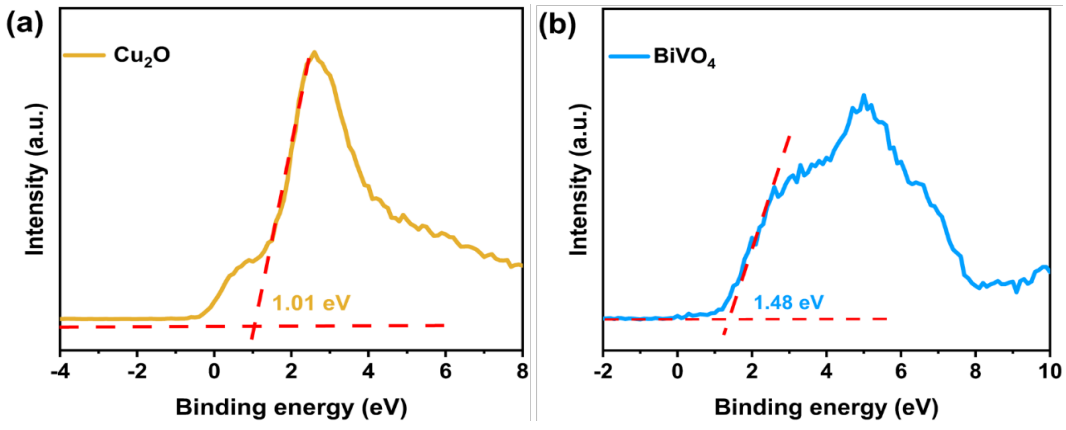

Fig. 5. XPS valence band spectra of (a) Cu_2O and (b) $BiVO_4$.

Fig. 6a displays the change in absorbance of TC with irradiation time over the pure Cu_2O, $BiVO_4$ and $Cu_2O/BiVO_4$ composites. The removal efficiency of pure $BiVO_4$ is 49.4% within 24 min, while the removal efficiency of pure Cu_2O is only 22.7%. It is clear that the degradation efficiency of the $Cu_2O/BiVO_4$ composites with different mass ratios is higher than

that of $BiVO_4$ and Cu_2O. This can be explained by the formation of a p-n heterojunction between $BiVO_4$ and Cu_2O, which effectively inhibits the recombination of charge carriers. With increasing $BiVO_4$ content, the photocatalytic activity of the prepared $Cu_2O/BiVO_4$ composites improves gradually, and Cu_2O:$BiVO_4$ (1:3) exhibits the highest degradation efficiency of 78.9% within 24 min. Additionally, the degradation rate of TC can be fitted by the pseudo-first-order kinetic model. As shown in Fig. 6b, the degradation process over all photocatalysts conforms to the pseudo-first-order kinetic. The degradation rate constant of TC for Cu_2O:$BiVO_4$ (1:3) is 0.06292 min^{-1}, which is 2.2 and 7.8 times that of $BiVO_4$ (0.02863 min^{-1}) and Cu_2O (0.00803 min^{-1}), respectively.

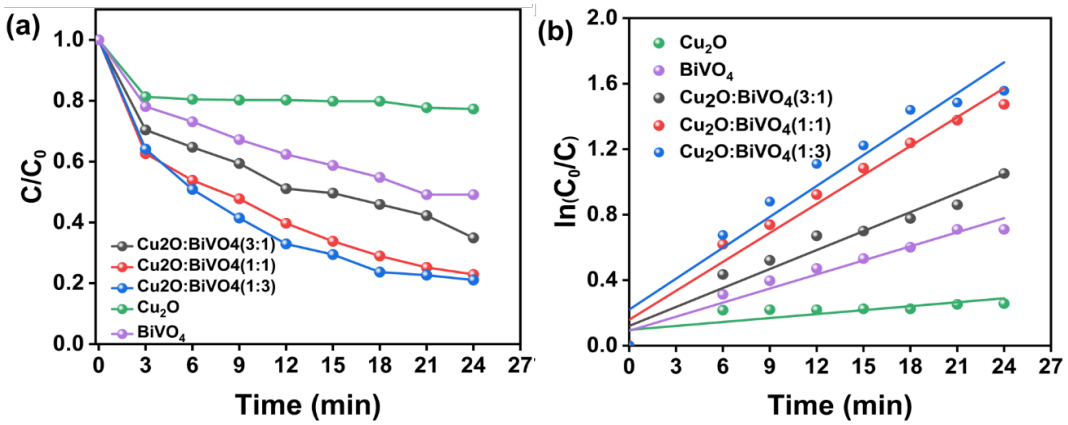

Fig. 6. (a) Photocatalytic activity and (b) corresponding kinetic curves of all samples for TC degradation.

The photocatalysis mechanism of the p-n $Cu_2O/BiVO_4$ heterojunction is proposed in Fig. 7. Under simulated solar illumination, both Cu_2O and $BiVO_4$ semiconductor can be excited to yield photogenerated carriers.

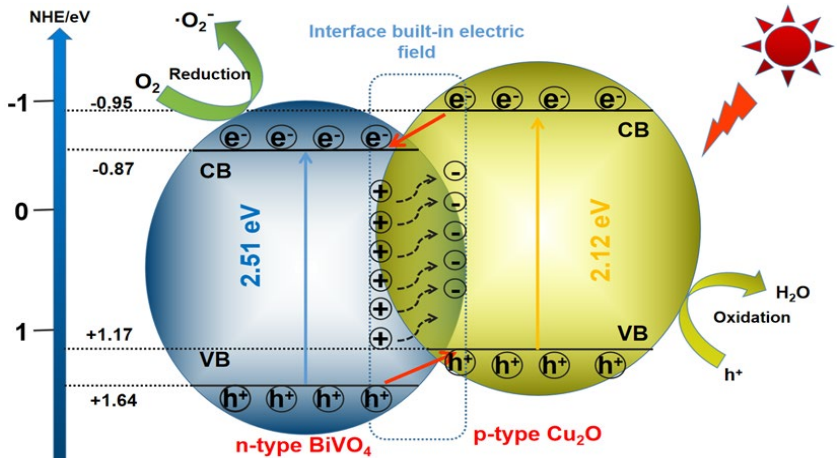

Fig. 7. Photocatalysis mechanism of p-n $Cu_2O/BiVO_4$ heterojunction.

When the p-type Cu_2O semiconductor is in contact with the n-type BiVO4 semiconductor, the built-in electric field becomes the driving force to separate the photogenerated electron-hole pairs. The electrons in the CB move from Cu_2O to $BiVO_4$ while the holes in the VB transfer from $BiVO_4$ to Cu_2O, which leads to a downward shift of the Fermi level in the Cu_2O and an upward shift of the Fermi level in the $BiVO_4$ until a pseudo-equilibrium is reached [32]. Owing to the built-in electric field, the separation efficiency of electron-hole pairs at the $Cu_2O/BiVO_4$ interface has been greatly improved, resulting in superior photocatalytic performance.

4. Conclusion

In summary, star-like $BiVO_4$ was synthesized by a hydrothermal method and cubic Cu_2O was prepared by the chemical reduction of copper sulfate. $Cu_2O/BiVO_4$ p-n heterojunction with different mass ratios was synthesized via physical mixing. Compared with pure Cu_2O and $BiVO_4$, the as-prepared $Cu_2O/BiVO_4$ composites showed superior photocatalytic activity for the degradation of TC. Among them, Cu_2O:$BiVO_4$ (1:3) catalyst exhibited the highest degradation efficiency of 78.9% within 24 min. The enhanced photoactivity was attributed to the formation of p-n heterojunction between $BiVO_4$ and Cu_2O, which facilitate the separation of carriers. It is expected that the $Cu_2O/BiVO_4$ composites can be used as a promising photocatalyst for wastewater treatment.

Acknowledgements

This work was supported by Sichuan Science and Technology Program (2023YFG0229).

References

[1] P. Valitalo, A. Kruglova, A. Mikola, R. Vahala, International Journal of Hygiene and Environmental Health 220, 558-569 (2017); http://dx.doi.org/10.1016/j.ijheh.2017.02.003
[2] M. F. Li, Y. G. Liu, G. M. Zeng, N. Liu, S. B. Liu, Chemosphere 226, 360-380 (2019); https://doi.org/10.1016/j.chemosphere.2019.03.117
[3] D. L. Cheng, H. H. Ngo, W. S. Guo, S. W. Chang, D. D. Nguyen, Y. W. Liu, Q. Wei, D. Wei, Journal of Hazardous Materials 386, 121682-121693 (2019); https://doi.org/10.1016/j.jhazmat.2019.121682
[4] F. Yu, Y. Li, S. Han, J. Ma, Chemosphere 153, 365-385 (2016); http://dx.doi.org/10.1016/j.chemosphere.2016.03.083
[5] M. J. F. Calvete, G. Piccirillo, C. S. Vinagreiro, M. M. Pereira, Coordination Chemistry Reviews 395, 63-85 (2019); https://doi.org/10.1016/j.ccr.2019.05.004
[6] G. Z. Fang, Z. F. Liu, C. C. Han, Applied Surface Science 515, 146095 (2020); https://doi.org/10.1016/j.apsusc.2020.146095
[7] P. Chatchai, S. Y. Kishioka, Y. Murakami, A. Y. Nosaka, Y. Nosaka, Electrochimica Acta 55, 592-596 (2010); http://dx.doi.org/10.1016/j.electacta.2009.09.032

[8] S. C. Hu, F. Zhou, L. Z. Wang, J. L. Zhang, Catalysis Communications 12, 794-797 (2011); http://dx.doi.org/10.1016/j.catcom.2011.01.027
[9] L. Z. Li, B. Yan, Journal of Non-Crystalline Solids 355, 776-779 (2009); http://dx.doi.org/10.1016/j.jnoncrysol.2009.04.003
[10] R. L. Liu, H. Y. Ye, X. P. Xiong, H. Q. Liu, Materials Chemistry and Physics 121, 432-439 (2010); http://dx.doi.org/10.1016/j.matchemphys.2010.02.002
[11] M. Agrawal, S. Gupta, A. Pich, N. E. Zafeiropoulos, M. Stamm, Chemistry of Materials 21, 5343-5348 (2009); http://dx.doi.org/10.1021/cm9028098
[12] K. Z. Lv, J. Li, X. X. Qing, W. Z. Li, Q. Y. Chen, Journal of Hazardous Materials 189, 329-335 (2011); http://dx.doi.org/10.1016/j.jhazmat.2011.02.038
[13] N. Wetchakun, S. Chaiwichain, B. Inceesungvorn, K. Pingmuang, S. Phanichphant, A. I. Minett, J. Chen, ACS Applied Materials & Interfaces 4, 3718-3723 (2012); http://dx.doi.org/10.1021/am300812n
[14] H. S. M. Abd-Rabboh, M. Benaissa, M. S. Hamby, M. A. Ahmed, M. Glal, Optical Materials 114, 110761 (2021); https://doi.org/10.1016/j.optmat.2020.110761
[15] B. Nikoobakht, J. Bonevich, A. Herzing, The Journal of Physics Chemistry C 115, 9961-9969 (2011); https://dx.doi.org/10.1021/jp201595a
[16] M. Zhou, Z. Guo, Z. F. Liu, Applied Catalysis B:Environmental 260, 118213 (2020); https://doi.org/10.1016/j.apcatb.2019.118213
[17] M. Liu, L. C. Zheng, J. L. Deng, J. Gao, K. R. Su, X. L. Sheng, J. He, D. Q. Feng, L. Guo, C. Z. Chen, Y. Li, Journal of Alloys and Compounds 931, 167584 (2023); https://doi.org/10.1016/j.jallcom.2022.167584
[18] C. Y. Toe, Z. K. Zheng, H. Wu, J. Scott, R. Amal, Y. H. Ng, Angewandte Chemie International Edition 57, 13613-13617 (2018); http://dx.doi.org/10.1002/anie.201807647
[19] J. W. Li, Z. L. Sun, M. Z. He, D. Gao, Y. T. Li, J. J. Ma, Inorganic Chemistry Communications 138, 109200 (2022); https://doi.org/10.1016/j.inoche.2022.109200
[20] H. L. Dou, L. Chen, S. H. Zheng, Y. P. Zhang, G. Q. Xu, Materials Chemistry and Physics 214, 482-488 (2018); https://doi.org/10.1016/j.matchemphys.2018.04.071
[21] X. N. Li, D. Q. Wei, L. Ye, Z. H. Li, Inorganic Chemistry Communications 104, 171-177 (2019); https://doi.org/10.1016/j.inoche.2019.04.012
[22] S. Y. Lee, H. J. Jung, N. K. Kim, H. S. Oh, B. K. Min, Y. J. Hwang, Journal of the American Chemical Society 140, 8681-8689 (2018); https://doi.org/10.1021/jacs.8b02173
[23] Y. A. Wu, I. McNulty, C. Liu, K. C. Lau, Q. Liu, A. P. Paulikas, C. J. Sun, Z. H. Cai, J. R. Guest, Y. Ren, V. Stamenkovic, L. A. Curtiss, Y. Z. Liu, T. Rajh, Nature Energy 4, 957-968 (2019); https://doi.org/10.1038/s41560-019-0490-3
[24] Q. K. Fan, X. Zhang, X. H. Ge, L. C. Bai, D. S. He, Y. T. Qu, C. C. Kong, J. L. Bi, D. W. Ding, Y. Q. Cao, X. Z. Duan, J. Wang, J. Yang, T. Wu, Advanced Energy Materials 11, 2101424 (2021); https://doi.org/10.1002/aenm.202101424
[25] Y. Q. Liu, Y. L. Xu, D. J. Zhong, H. Y. Yao, Y. D. Zeng, N. B. Zhong, H. Luo, Colloids and Surfaces A: Physicochemical and Engineering Aspects 612, 125941 (2021); https://doi.org/10.1016/j.colsurfa.2020.125941
[26] Y. Liu, J. J. Kong, J. L. Yuan, W. Zhao, X. Zhu, C. Sun, J. M. Xie, Chemical Engineering Journal 331, 242-254 (2018); http://dx.doi.org/10.1016/j.cej.2017.08.114
[27] X. Wang, Z. C. Guan, P. Jin, Y. Y. Tang, G. L. Song, G. K. Liu, R. G. Du, Corrosion Science

157, 247-255 (2019); https://doi.org/10.1016/j.corsci.2019.05.034
[28] M. Mousavi-Kamazani, Ultrasonics Sonochemistry 58, 104636 (2019); https://doi.org/10.1016/j.ultsonch.2019.104636
[29] Q. Yuan, L. Chen, M. Xiong, J. He, S. L. Luo, C. T. Au, S. F. Yin, Chemical Engineering Journal 255, 394 (2014); http://dx.doi.org/10.1016/j.cej.2014.06.031
[30] Z. D. Zhang, X. Y. Chen, S.H. Chen, Q. Dong, X. Y. Zhang, A. Jiang, D. F. Zhang, Y. L. Di, T. S. Li, Optical Materials 133, 113081 (2022); https://doi.org/10.1016/j.optmat.2022.113081
[31] T. T. Wang, J. J. Cai, J. Y. Zheng, K. K. Fang, I. Hussain, D. Z. Husein, Journal of Materials Science and Technology 19, 5017-5036 (2022); https://doi.org/10.1016/j.jmrt.2022.06.177
[32] E. Aguilera-Ruiz, U. M. Garcia-Perez, M. de la Garza-Galvan, P. Zambrano-Robledo, B. Bermudez-Reyes, J. Peral, Applied Surface Science 328, 361-367 (2015); http://dx.doi.org/10.1016/j.apsusc.2014.12.059